DOI: 10.1002/agj2.21611

ORIGINAL ARTICLE

Biometry, Modeling, and Statistics



Check for updates

Representing cropping systems with the MEMS 2 ecosystem model

Yao Zhang¹ Alison E. King² Emma Hamilton² M. Francesca Cotrufo²

¹Natural Resources Ecology Laboratory, Colorado State University, Fort Collins, Colorado, USA

²Department of Soil and Crop Sciences. Colorado State University, Fort Collins, Colorado, USA

Correspondence

Yao Zhang, Natural Resources Ecology Laboratory, Colorado State University, Fort Collins, CO 80523, USA.

Email: yao.zhang@colostate.edu

Assigned to Associate Editor Stephen Del Grosso

Funding information

National Science Foundation Division of Environmental Biology, Grant/Award Number: 2016003; Shell United States, Grant/Award Number: 4550183252; U.S. Department of Energy Advanced Research Projects Agency - Energy, Grant/Award Number: DE-FOA-00001565

Abstract

Croplands have been the focus of substantial investigation due to their considerable potential for sequestering carbon. Understanding the potential for soil organic carbon (SOC) sequestration and necessary management strategies will be enabled with accurate process-based models. Accurately representing crop growth and agricultural practices will be critical for realistic SOC modeling. The MEMS 2 model incorporates a current understanding of SOC formation and stabilization, measurable SOC pools, and deep SOC dynamics and is seen as a highly promising tool to inform management intervention for SOC sequestration. Thus far, MEMS 2 has been developed to represent grasslands. In this study, we further developed MEMS 2 to model annual grain crops and common agricultural practices, such as irrigation, fertilization, harvesting, and tillage. Using four Ameriflux sites, we demonstrated an accurate simulation of crop growth and development. Model performance was strong for simulating aboveground biomass (index of agreement [d] range of 0.89–0.98) and green leaf area index (d from 0.90 to 0.96) across corn, soybean, and winter wheat. Good agreement with observations was also achieved for net ecosystem CO₂ exchange (d from 0.90 to 0.96), evapotranspiration (d from 0.91 to 0.94), and soil temperature (d of 0.96), while discrepancy with the available soil water content data remain (d from 0.14 to 0.81 at four depths to 100 cm). While we will continue model testing and improvement, MEMS 2 (version 2.14) has now demonstrated its ability to effectively simulate the growth of common grain crops and practices.

INTRODUCTION

Soil organic carbon (SOC) comprises a large portion of and therefore exerts a large influence on—the active carbon (C) in the global C cycle (Janzen, 2004). Arable lands,

Abbreviations: AI, artificial intelligence; ET, evapotranspiration; GLAI, green leaf area index; MAOC, mineral-associated organic carbon; NEE, net ecosystem CO₂ exchange; NPP, net primary production; POC, particulate organic carbon; RMD, relative mean difference; RRMSE, relative root mean square error; SOC, soil organic carbon; ST, soil temperature; SWC, soil water content.

which account for $\sim 12\%$ of the Earth's ice-free land area (Ramankutty et al., 2008), have historically acted as a source for atmospheric C due to the loss of SOC upon conversion from native vegetation to arable agriculture (Guo & Gifford, 2002; Sanderman et al., 2017). In addition to these historic SOC losses, ongoing soil C emissions contribute to about 32% of total global greenhouse gas emissions from food systems (Crippa et al., 2021). SOC loss threatens food security, given the role of SOC in supporting crop yields (Amelung et al., 2020; Oldfield et al., 2019). While arable lands, if managed appropriately, have the potential to recover some of this SOC

This is an open access article under the terms of the Creative Commons Attribution-NonCommercial License, which permits use, distribution and reproduction in any medium, provided the original work is properly cited and is not used for commercial purposes.

© 2024 The Author(s). Agronomy Journal published by Wiley Periodicals LLC on behalf of American Society of Agronomy.

(Paustian et al., 2016), estimates attempting to quantify this potential reveal enormous uncertainty, with global estimates of soil C sequestration potential ranging from 0.06 to 0.61 Pg C year⁻¹ (Lal et al., 2018). This wide range of estimated SOC sequestration in arable lands reflects, in part, the complexity of the C cycle and ongoing challenges in constraining the behavior of soil C in tools used to generate these forecasts.

Ecosystem models are a key tool to forecast the response of SOC to different agricultural management scenarios (Dondini et al., 2009; Launay et al., 2021; Lugato et al., 2014). In a rapidly increasing agricultural soil C market, model forecasts of agricultural SOC can strengthen hybrid approaches to measurement, reporting, and verification to constrain estimates of SOC gains from improved management (Oldfield et al., 2022). Models representing up-to-date understandings of SOC can also serve as tools for scientific inquiry and hypothesis-testing. Both the robustness of model predictions and utility for scientific inquiry, however, depend on informing models with current understandings of the mechanisms governing SOC and its constituent components. While many existing process-based ecosystem models simulate arable lands (e.g., CENTURY [Parton et al., 1987], RothC [Coleman & Jenkinson, 1996], DayCent [Parton et al., 1998], DNDC [Li et al., 1992], and SALUS [Basso et al., 2006]), these models rely on a conceptual framework of SOC as composed of pools that cannot be measured, hindering model verification and calibration. Many newer soil C models that incorporate measurable SOC pools have been developed thus far for forests (Sulman et al., 2017; Wang et al., 2020; Wieder et al., 2014; Yu et al., 2020), grasslands (F. H. M. Tang et al., 2019; Zhang et al., 2021), or a combination of natural systems (Abramoff et al., 2022; Tifafi et al., 2018). While a small number of these models use a foundation of observations from agricultural systems (Abramoff et al., 2022; Woolf & Lehmann, 2019), there is still a need to develop models that represent measurable SOC pools in order to represent agricultural management and crop species, thereby meeting the modeling needs for croplands outlined above.

Simulating SOC in arable lands with process-based modeling relies on an accurate representation of crop growth, as unharvested portions of crops provide the plant C inputs that maintain SOC. Models designed to estimate crop growth, usually with a focus on yield (Kollas et al., 2015), typically perform well for this purpose by explicitly representing biophysical processes of crop development, such as biomass production and partitioning, leaf area, nitrogen (N) and water uptake, anthesis, and harvesting (Abrahamsen & Hansen, 2000; Jones et al., 2003; Keating et al., 2003; Stöckle et al., 2003). To simulate crop growth, crop models are developed with in-season measurements to validate crop development, including biomass and leaf area; when available, net ecosystem exchange can aid in constraining soil-vegetationatmosphere C fluxes (Friend et al., 2007; Revill et al., 2019).

Core Ideas

- The MEMS 2 model was developed to simulate annual crops and agricultural management.
- Validation showed the MEMS 2 can accurately represent the growth and production of three major crops at four sites.
- The simulated soil carbon pools were within the range of reported values from field studies.

These models also represent crop responses to management, including N fertilizer, irrigation, and tillage. Currently, there exists a gap between these crop growth models and measurable SOC pools, as models so far have not been developed to provide comprehensive simulation of the crop species and management choices that moderate measurable SOC pools in arable lands.

The MEMS 2.0 model (Zhang et al., 2021) is an ecosystem soil C and N model that integrates multiple foundational advances in our understanding of C and N dynamics between plants, microbes, soil, and the atmosphere. The MEMS model simulates and has been validated (Zhang et al., 2021) against measured SOC pools of particulate organic carbon (POC) and mineral-associated organic carbon (MAOC), which have been proposed as distinct SOC pools with contrasting mechanisms of formation and stabilization resulting in different turnover times and vulnerability to change (Cotrufo & Lavallee, 2022). These pools can be isolated through established, laborintensive laboratory physical fractionation methods, which are scalable to higher throughput via FTIR (Ramírez et al., 2021), and artificial intelligence (AI) approaches (Cotrufo et al., 2019; Lugato et al., 2021). The MEMS model is depth-resolved with user-defined soil layers. Therefore, the model can simulate subsoil C stocks and has the capability to simulate finely-resolved soil profile increments near the surface, where responses to management commonly occur, which in turn are important for soil functioning (Franzluebbers, 2002; VandenBygaart et al., 2011). The MEMS model also simulates N dynamics, aiding in the representation of soil microbial and SOC formation and stabilization process. These representations include explicit microbial pools, microbial carbon use efficiency controlled by input C:N ratios (Cotrufo et al., 2013; Soares & Rousk, 2019), distinct input point of entry in bulk and rhizosphere soils (Sokol et al., 2019), the two pathways of POC and MAOC formation (Cotrufo et al., 2015), distinct processes of in vivo and ex vivo pathways of soil C processing and MAOC formation (Liang et al., 2017), matrix control on MAOC saturation, as well as MAOC separation into stable and exchangeable pools (Kleber et al., 2007), providing a modern model structure that retains the capacity to be adapted to new advances in ecosystem and soil

biogeochemistry. While MEMS 2.0 was initially presented for grasslands, given their importance for global terrestrial C stocks and value as model systems (Zhang et al., 2021), MEMS 2.0 has not previously been developed to represent croplands.

There are many existing crop models that have accurately simulated crop growth and yield. We studied and tested several of the leading models (e.g., Ritchie & Otter, 1985; Wolf, 2012), selecting and adapting key methods and equations to develop an annual crop submodel for our purposes. Our goal was to strike a balance between simplicity in model structure (one general template for all annual crops with minimal parameters) and data requirements, yet still achieve good accuracy in representing crop processes. This approach to develop cropland representation aligns with the overarching philosophy of the MEMS model development, which is to parsimoniously represent measurable C and N pools and fluxes to achieve accurate simulations of ecosystem processes. Here, we show the development of the MEMS model (version 2.14) for the simulation of agricultural crops such as corn (Zea mays), soybean (Glycine max), and wheat (Triticum aestivum). These three major agricultural crops together are planted on over 500 million ha globally (FAOSTAT, 2021), or approximately one-third of arable land (Ramankutty et al., 2008), making them clear priorities for model development. We parameterize the model using data from three sites in eastern Nebraska and a site in northern Oklahoma. Although simulation of SOC, POC, and MAOC in response to land conversion to cropland and subsequent implementation of no-till were not the focus of this study, we also present model performance for these SOC pools to evaluate how model simulations align with general, expected patterns in SOC dynamics.

2 | MATERIALS AND METHODS

2.1 | Model description

We further developed the MEMS model to represent annual grain crop growth and agricultural management. The soil modules of the model described in Zhang et al. (2021) have not been changed. Here, we describe the new key developments related to cropland representation.

2.1.1 | Daily net primary production and crop growth

The plant production submodel in our model uses the simple radiation use efficiency approach (Zhang, Suyker, et al., 2018).

$$NPP_i = RUE \times PAR_i \times CC_i \times T_i \times S_i \times CF_i \qquad (1)$$

where NPP_i is the net primary production (g C m⁻²) on day *i*. RUE is the radiation use efficiency, which is kept as constant for the entire growing season for each crop. PAR_i is the photosynthetic radiation (MJ m⁻² day⁻¹) on day *i*. CC_i is the canopy cover on day *i*, ranging from 0 to 1. T_i is the temperature effect (ranges from 0 to 1). S_i is the stress factor on day *i* including environmental stresses such as drought and nutrient deficiency (ranges from 0 to 1, with 1 indicating no stress and 0 indicating complete stress).CF_i is the atmospheric CO₂ fertilization effect using a simple method from Soltani and Sinclair (2012). Plant maintenance respiration, growth respiration, and respiration from symbiotic N fixation were calculated using methods from the GECROS model (Yin & van Laar, 2005).

Daily net primary production (NPP) is allocated to leaf, stem, seed, coarse root, fine root, and exudate on a daily time step. The partitioning of NPP is based on user-defined linear curves as a function of plant phenology (Zhang et al., 2021).

The model currently simulates N as the sole plant nutrient. Nitrogen in the soil is represented in mineral and organic forms. Plants and soil microbes compete for mineral forms of N, as described in Zhang et al. (2021). The crop N demand, allocation, and translocation within the plant were calculated using the methods from the LINTUL model (Wolf, 2012). Symbiotic N fixation by legumes was modeled as in the GECROS model (Yin & van Laar, 2005).

2.1.2 | Leaf and green leaf area index development

The leaf development uses the method described in Zhang, Suyker et al. (2018), which relies on the concept of green leaf weight ratio (a function of phenology). The expansion of leaves is a result of the allocation of NPP to leaves, which follows a three-stage curve (Zhang, Suyker, et al., 2018). The senescence of leaves is determined by the daily maximum green leaf area index (GLAI) based on the expected green leaf weight ratio for each day; at any day when the existing GLAI value exceeds the daily maximum GLAI, the amount of leaf biomass in excess will be considered in senescence. Daily GLAI is calculated from leaf biomass using the specific leaf area (a user input parameter).

2.1.3 | Phenology

We adopted the phenology calculations used in Yin and van Laar (2005). The phenology of development is based on the daily accumulation of heat units. The method of photoperiod effect on heat units is derived from Soltani and Sinclair (2012), and the vernalization effect is derived from the

CERES-wheat model (Ritchie & Otter, 1985). In the MEMS 2.14 model, the phenology stage is represented numerically between 0 and 2, with 0 for emergence, 1 for anthesis, and 2 for physiological maturity.

2.1.4 | Evapotranspiration

The MEMS 2.14 model estimates evapotranspiration (ET) using a method comparable to the FAO approach (Allen et al., 1998). This involves first calculating the reference ET for well-watered turfgrass using daily meteorological data, then multiplying by crop-specific coefficients. Both the standardized Penman-Monteith method (Allen et al., 1998) and the Hargreaves method (Hargreaves & Allen, 2003) are available for the calculation of the reference ET in MEMS 2.14. The Hargreaves method only requires daily maximum and minimum air temperatures, while the Penman-Monteith method needs solar radiation, wind speed, and relative humidity as input. The MEMS 2.14 model uses a dynamic crop coefficient method based on GLAI to calculate potential ET for specific crops (Zhang, Suyker, et al., 2018). The partitioning of evaporation and transpiration is based on crop canopy cover (Raes et al., 2009). The soil water submodel (Ross, 2003) calculates the actual evaporation and transpiration based on soil water potential and root distribution. The model simulates rooting depth increase for annual crops from planting to harvest, with root distribution simulated as described in Robertson et al. (2019) and Zhang et al. (2021). The effect of surface litter on evaporation is calculated using a simple method from the DayCent model (Parton et al., 1998).

2.1.5 | Soil water

The MEMS 2.14 model uses a soil-water model from Ross (2003). In the earlier version of the MEMS model (Zhang et al., 2021), the soil hydraulic parameters (Brooks & Corey, 1964) were either provided by users or estimated by a pedotransfer method from Saxton and Rawls (2006), with field capacity at -33 kPa and wilting point at -1500 kPa. These parameters would then be fixed for the entire simulation run. We improved the model by adding an option to allow the model to dynamically update these hydraulic parameters after a tillage event or a significant change of SOC within a soil layer. We also added a pedo-transfer method from Bagnall et al. (2022), which was shown to be more sensitive to SOC change. The bottom boundary condition of the soil can be set as free drainage, constant head, seepage face, or zero flux. The soil water submodel can represent the slow drainage of poorly drained soils. If present, tile drainage can be modeled by setting the bottom boundary condition to the seepage face (Rassam et al., 2018).

2.1.6 | Management practices

We added agricultural practices to this version of the MEMS model. These management events can be specified in the daily schedule input file. The model can simulate either fixed amounts of irrigation (user-specified) or automatic irrigation events, which are based on the root zone water availability (Allen et al., 1998); drip irrigation is currently not supported as the three-dimensional wetting pattern and root uptake dynamics cannot be easily captured by one-dimensional models such as ours. Mineral N fertilization events are represented by the addition of ammonium and/or nitrate to the soil surface or at a user-specified depth. A harvest event can remove all or a fraction of crop grain and residue.

We implemented cultivation and tillage in this model version. Depending on the type of cultivation, live and standing dead crop biomass can be transferred to surface and soil litter pools. Surface residue can be incorporated into the soil. We also implemented soil mixing of the soil litter and organic matter pools, and mineral N for the soil layers within the tillage depth. A user-defined fraction represents the mixing efficiency (Williams & Izaurralde, 2010) of the pools in the soil layers, which are evenly mixed, and the pools are redistributed accordingly.

Similarly, model users can change the soil bulk density for any soil layer on a specific day. This option allows the users to account for the soil compression and expansion effects on the calculated C and N stock changes at certain depths over time. In the model, soil layer depths are fixed during a simulation. However, a bulk density change results in a movement of SOM pools from one layer to another (which can be seen as redefining the depths after a bulk density change; the soil surface is always a depth of 0 cm as a reference). We plan to further develop the model to represent a dynamic bulk density change due to tillage.

Organic amendment added to the soil surface, such as compost or manure, is modeled as the addition of C and N to a set of three surface litter pools (soluble, hydrolyzable, and unhydrolyzable). These pools are separated from the existing litter pools of the plant. As a result, the changes of C and N of the organic amendment can be tracked and compared with observations. In contrast, the applied organic amendment to subsurface soil will be immediately mixed with the root litter. The inorganic N added with the organic amendment can be simulated as a fertilization event on the same day.

2.2 | Experimental sites

Four sites from the AmeriFlux network (Novick et al., 2018) were chosen for model parametrization and validation. These sites were characterized by the availability of high-frequency measurements related to critical agricultural variables,

including crop leaf area index (LAI) and biomass (Zhang, Suyker, et al., 2018), rendering them well-suited for the rigorous assessment of simulated crop growth within the model framework. Three of the sites were companion sites growing corn and soybean under varying irrigation regimes. The fourth site planted continuous winter wheat. Following is a detailed description of these sites.

2.2.1 | The Mead, NE sites

2332

The US-Ne1 (Suyker, 2023a), US-Ne2 (Suyker, 2023b), and US-Ne3 (Suyker, 2023c) sites are located within 1.6 km of each other at the University of Nebraska Agricultural Research and Development Center near Mead, NE. Detailed information about the sites can be found in Suyker and Verma (2009). The soils at these sites are deep silty clay loams with very little slope. The experiments started in 2001, with different management applied at the three sites. US-Ne1 is irrigated by a center pivot system and planted continuous maize. US-Ne2 is also irrigated but was planted with a maize-soybean rotation from 2001 to 2008 and changed to continuous maize in 2009. US-Ne3 is a rainfed field with maize-soybean rotation. At the beginning of the experiment in 2001, all sites were tilled. After 5 years of no-till, the US-Ne1 site was converted to conservation tillage. Tillage was implemented at the US-Ne2 site in 2010, while the US-Ne3 site remained under no-till. Management details are recorded and available at the AmeriFlux online database.

As part of the AmeriFlux network, eddy covariance towers (to measure CO₂, H₂O, and energy fluxes) were installed at each site (Suyker & Verma, 2009). Soil moisture sensors were placed at 10-, 25-, 50-, and 100-cm depth, and soil temperature (ST) data are available at 2- and 4-cm depth. Six 20 m by 20 m intensive measurement zones were established in each field to measure aboveground biomass and leaf area index using a destructive method (Grant et al., 2007). Grain yield data are acquired from the combined harvest of each field.

2.2.2 | The US-Pon site

The US-Pon site (Verma, 2016) is located near Ponca City, OK (Hanan et al., 2002). The site was planted with winter wheat continuously from 1996 to 2000. The upper 0.6 m of the soil profile comprises a silty clay loam, while beneath lies a thick clay horizon. Aboveground biomass and GLAI were also measured using destructive methods. More detailed information regarding management is not available on this site.

2.3 | Simulation setup and parameterization

The input files for this simulation were prepared using the soil characteristics, historical weather information, and agricultural management data of these sites from Zhang, Suyker et al. (2018). While detailed management information was available for the Mead, NE, sites, data specific to the Ponca, OK site was lacking. Thus, management practices commonly used in the surrounding region were assumed for simulating the winter wheat grown at the Ponca, OK site (Zhang, Suyker, et al., 2018).

To initialize the model, a 900-year simulation of native grassland was conducted to allow SOC to reach equilibrium. For the Mead, NE sites, corn—soybean rotation under conventional tillage was simulated from 1900 to establish realistic initial soil C levels at the start of the experiment. No-till practices were modeled beginning in 1990, reflecting documentation that the irrigated sites had been under no-till management for 10 years prior. Since details on irrigation system installation were unavailable, 1990 was assumed as the initiation year. For the Ponca, OK site, monocropped winter wheat with conventional tillage was simulated from 1900 through the experimental period.

Crop parameters were based on measured data and values from the literature. Most crop parameters were either directly measured or previously documented when parameterizing another ecosystem model (Zhang, Suyker, et al., 2018). Thus, manual calibration was used to minimize relative root mean square error (RRMSE) for GLAI and biomass simulations using measured data from 2022 for the Mead, NE sites and data from 1997 for the Ponca, OK site. The rest of the data from these sites were used for validation. Thus, the validation data were not completely independent. The calibrated crop parameters can be found in Table S1. The decomposition-related parameters were kept at default values from the grassland parameterization (Zhang et al., 2021).

2.4 | Model validation

Model validation was performed by comparing simulated outputs to measured data. The GLAI and biomass simulations were evaluated against the observed values that were excluded from calibration. Additional model evaluations were conducted using measured crop yield, net ecosystem CO₂ exchange (NEE), ET, soil water content (SWC), and ST data from the Mead, NE sites. Comparisons between simulated and observed SOC were also performed, but were not considered formal validation since detailed historical management information prior to the experiments, which would be

needed to capture SOC dynamics, was unavailable. The following statistical metrics were used to quantify the model's performance:

1. Index of agreement (d)

$$d = 1 - \frac{\sum_{i=1}^{n} (P_i - O_i)^2}{\sum_{i=1}^{n} (|P_i - \bar{O}| + |O_i - \bar{O}|)^2}$$
(2)

2. Coefficient of determination (R^2)

$$R^{2} = 1 - \frac{\sum_{i=1}^{n} (Pi - Oi) 2}{\sum_{i=1}^{n} (Oi - \bar{O}) 2}$$
 (3)

3. Relative root mean square error (RRMSE)

RRMSE =
$$\frac{1}{\bar{O}} \sqrt{\frac{1}{n} \sum_{i=1}^{n} (Pi - Oi) 2}$$
 (4)

4. Relative mean difference (RMD)

$$RMD = \frac{1}{\bar{O}} \left(\bar{P} - \bar{O} \right) \tag{5}$$

3 | RESULTS AND DISCUSSION

3.1 | Crop growth and biomass production

3.1.1 | Aboveground biomass and LAI

The Mead, NE sites' frequent measurements of biomass and LAI are ideal for rigorous calibration and validation of crop growth models. Although different varieties of corn and soybean were planted each year, our objective was not to parameterize the model for each individual variety. This type of parameterization would limit the utility of the model to real-world applications, where information on crop variety is often not accessible. Therefore, we followed a more practical approach in establishing a general parameterization of crops for the region (Zhang et al., 2020).

Our model validation compared the modeled and measured aboveground biomass of corn and soybean crops at the three AmeriFlux sites in Mead, NE, over 10 growing seasons (Figure 1). Despite using only one parameter set for each crop across varieties, our model accurately captured the rates of biomass accumulation for both crops, as evidenced by the high d (>0.96) and R^2 values (>0.88) and relatively low RRMSE and RMD values (Table 1). At US-Ne3, where the crops were not irrigated and experienced water stress during certain periods of the growing season, the modeled results showed similar reductions in biomass as the measurements, indicating the model accurately simulated the effect of water stress on crops.

However, in 2009, our model significantly underestimated the final crop biomass for US-Ne1 and US-Ne2 by 26% and 25%, respectively. Our analysis revealed that this underestimation was not due to water or nutrient stress. We suspect that the specific hybrid of corn used in 2009 was not represented by the parameter set (US-Ne1 and US-Ne2 used the same hybrid in 2009, but it was different from the one at US-Ne3 in 2009 or any other years at the sites).

To predict biomass accurately, it is necessary to first predict GLAI, as GLAI determines the amount of solar radiation intercepted by green leaves that can subsequently be used in photosynthesis. The MEMS 2.14 model successfully simulated changes in GLAI over the growing season for both corn and soybean (Table 1; Figure 2), with d values of 0.93 and 0.96 for corn and 0.90 for soybean for irrigated sites (US-Ne1 and US-Ne2), and 0.92 for corn and 0.91 for soybean for the rainfed site (US-Ne3). While these d statistics indicate overall strong model performance, the RRMSE and RMD values revealed that the model captured GLAI slightly better at the irrigated compared to rainfed sites (Table 1). This can be attributed to the overestimation of GLAI at the rainfed site, especially in 2003, 2008, 2010, and 2011. For the irrigated sites, the measurements of corn showed a general pattern where, after GLAI was reached, there was a slight decline before the late-season senescence. In contrast, the simple algorithm used in MEMS predicts GLAI to plateau during the summer months after the peak for corn. Nevertheless, the accuracy of the MEMS 2.14 model in predicting biomass and GLAI is similar to or better than reported values for other popular crop models and ecosystem models (Amiri et al., 2022; Archontoulis et al., 2014; Babel et al., 2019; Marek et al., 2017; Zhang, Hansen, et al., 2018).

The calibrated model also demonstrated good performance for winter wheat (Figure 3). However, the model fit for green aboveground biomass was not as strong as the total aboveground biomass (green and dead) for corn and soybean at the Mead, NE sites, with a d of 0.89, an R^2 of 0.66, an RRMSE of 0.85, and RMD of 0.24. The GLAI statistics were more favorable, with a d of 0.95, an R^2 of 0.91, an RRMSE of 0.43, and RMD of 0.24, though the model tended to slightly overpredict GLAI in 1999 and 2000. Winter wheat is planted in the fall and requires a vernalization period during cooler months in order to flower, which increases the difficulty of predicting its phenology and biomass production accurately (Fowler et al., 2014).

3.1.2 | Grain yield

While grain yield prediction is not a primary focus of most ecosystem models, accurate yield predictions are still crucial to represent cropping systems because grain harvest constitutes an export of C and nutrients from the field or ZHANG ET AL.

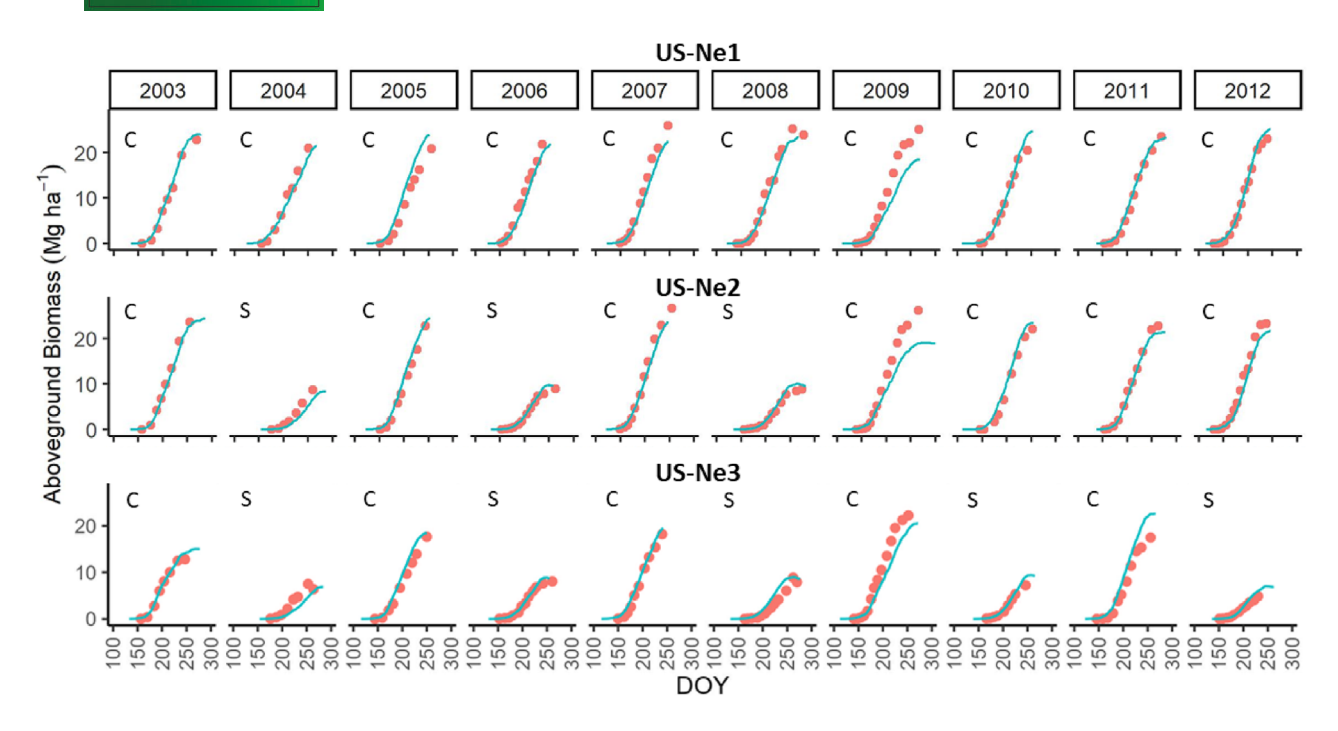


FIGURE 1 Comparison of simulated (lines) and measured (dots) aboveground biomass of the validation dataset at Mead, NE. Corn and soybean were denoted as C and S, respectively. US-Ne1, US-Ne2, and US-Ne3 are three sites from the AmeriFlux network.

TABLE 1 The statistics for model validation.

			Corn				Soybean		
		Aboveground biomass	GLAI	NEE	ET	Aboveground biomass	GLAI	NEE	ET
US-Ne1	d	0.98	0.93	0.95	0.94				
	R^2	0.94	0.77	0.84	0.79				
	RRMSE	0.22	0.32	-2.18	0.49				
	RMD	-0.02	0.04	0.79	-0.11				
US-Ne2	d	0.98	0.96	0.96	0.94	0.98	0.90	0.91	0.92
	R^2	0.95	0.86	0.86	0.80	0.93	0.69	0.73	0.77
	RRMSE	0.21	0.27	-1.50	0.49	0.27	0.57	7.19	0.56
	RMD	-0.05	0.09	0.41	-0.08	0.04	0.17	-1.50	-0.22
US-Ne3	d	0.97	0.92	0.95	0.93	0.96	0.91	0.90	0.91
	R^2	0.91	0.81	0.84	0.78	0.88	0.73	0.74	0.75
	RRMSE	0.27	0.42	-1.50	0.53	0.39	0.53	-138.76	0.58
	RMD	0.06	0.26	0.31	-0.17	0.12	0.20	3.46	-0.28

Note: The variables are daily values of aboveground biomass, green leaf area index (GLAI), net ecosystem exchange (NEE), and evapotranspiration (ET). US-Ne1 and US-Ne2 are irrigated, while US-Ne3 is rainfed.

Abbreviations: RMD, relative mean difference; RRMSE, relative root mean square error.

modeled system. Trustworthy model representations of grain yield also provide another avenue for model validation because grain yield data is often collected in cropping systems, whereas many other measurements related to crop growth (GLAI and NPP) may not be available. Grain yield can be used to estimate crop biomass production and NPP (Prince

et al., 2001), which can then be used to calibrate or validate ecosystem models (Zhang et al., 2020).

In this study, the modeled grain yield for corn and soybean generally agreed well with measurements (Figure 4), with a d of 0.66, an R^2 of 0.14, an RRMSE of 0.16, and an RMD of 0.02 for corn, except for 2009, which had an underprediction



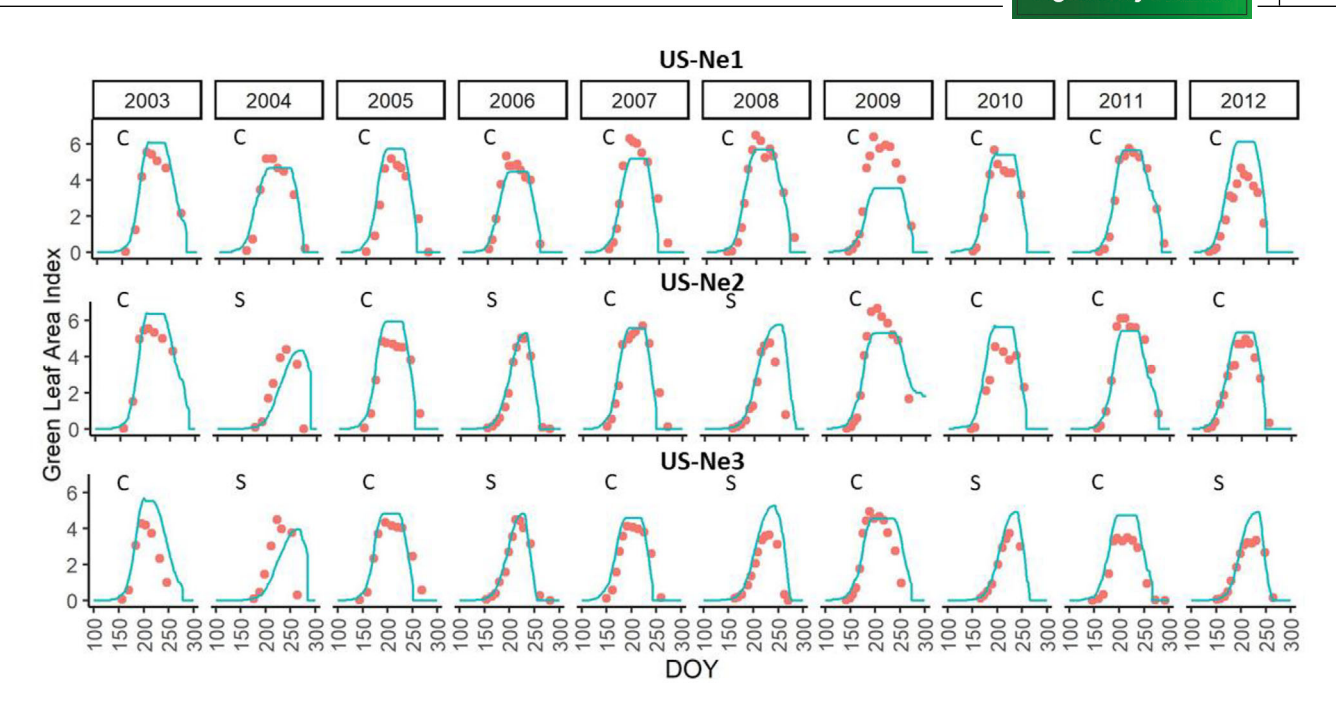


FIGURE 2 Comparison of simulated (lines) and measured (dots) green leaf area index of the validation dataset at Mead, NE. Corn and soybean were denoted as C and S, respectively. US-Ne1 and US-Ne2 are irrigated, while US-Ne3 is rainfed. DOY, day of year.

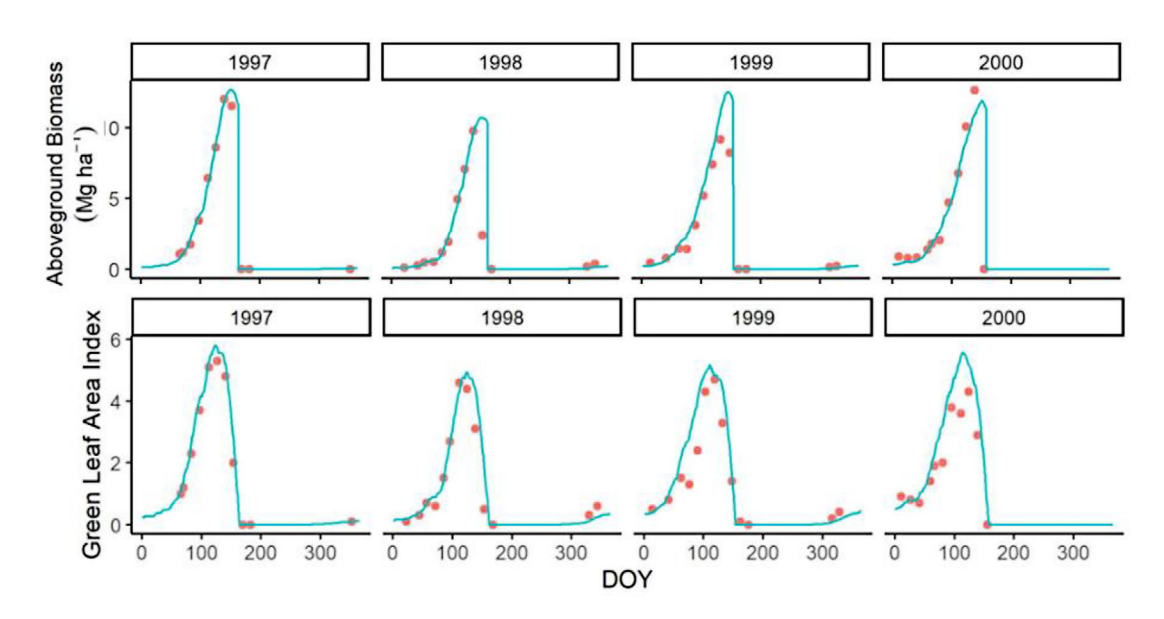


FIGURE 3 Comparison of simulated (lines) and measured (dots) green aboveground biomass and green leaf area index of winter wheat at the AmeriFlux US-Pon site in Oklahoma. The data from the year 1997 were used for calibration. DOY, day of year.

of 39% (the same year of substantial underestimation of biomass as discussed above). The statistics for soybean are better, with a d of 0.89, an R^2 of 0.74, an RRMSE of 0.11, and an RMD of 0.06. The measured yield of corn and soybean at the rainfed site US-Ne3 was lower than at the irrigated sites due to water stress, and the model accurately captured this effect of water stress for most years, leading to lower yield values at US-Ne3.

3.2 | Evapotranspiration, soil water content, and soil temperature

3.2.1 | Evapotranspiration and soil water content

During nongrowing periods, ET occurs only through the evaporation of water from surface residue and soil. Surface

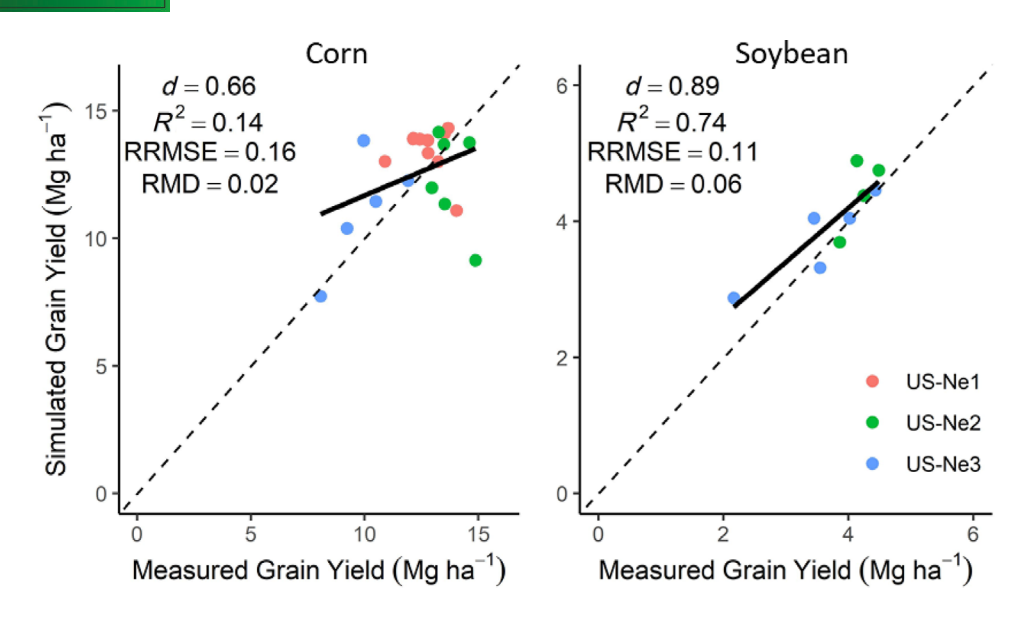


FIGURE 4 Comparison of simulated and measured grain yield of corn and soybean from the three AmeriFlux sites at Mead, NE. RMD, relative mean difference; RRMSE, relative root mean square error.

residue has a dual role in moderating ET, as it covers the bare soil surface and prevents soil water from evaporating but also intercepts a small amount of rain and provides a source of evaporation, especially between crop maturity and harvest. During growing periods, ET has been found to be closely related to crop canopy cover (Steduto et al., 2009), which can be calculated using GLAI (Zhang, Suyker, et al., 2018). As the model accurately predicted GLAI (Table 1; Figure 2), the modeled ET was also in good agreement with measurements from the eddy covariance towers at the Mead, NE sites (Table 1; Figures S1–S3). However, the simulated ET tended to be lower than the measured ET, as indicated by the negative RMD values (Table 1), with the largest bias observed for the rainfed site US-Ne3. The underestimation was mainly observed in the spring period (Figures S1–S3) where soil evaporation was the main source of ET. Soil evaporation is reduced by the crop residue on the soil surface, but this effect might not be accurately represented in the model. Another possibility for the underestimation is that the measurements themselves in the spring periods were biased. The model calculates water mass balance on a daily basis, and simulated SWC was found to be highly consistent with measurements (Figures S4–S15), especially for the top 10 cm of soil, as shown in Figures S4–S6. If the model were to increase soil evaporation to match the measured values, simulated SWC would decrease to maintain water balance, resulting in an underestimation of SWC.

Although the d and R^2 values of the simulated SWC were not as high as those of other variables (Table 2), the RRMSE and RMD were relatively small. The soil water retention parameters were estimated using the Saxton method (Saxton & Rawls, 2006), which is known for biased predictions

in some soil types. Some clear bias of SWC field capacity can be observed compared with the measured values, especially for deeper soil layers (e.g., underestimation in Figures \$13 and \$14). What challenges the calibration of the model, however, is that the accuracy of the SWC measurements themselves may not be perfect, as sensor data appear unrealistic in certain cases. For example, in 2006 at US-Ne1, the SWC at 10 and 25 cm was substantially shifted to a lower range of values compared to other years or the same year at other sites (as seen in Figures \$4 and \$7). Nevertheless, overall, the model performed well in predicting both ET and soil water. As soil water is critical for soil biological processes, the accuracy of SWC and ET predictions largely affects the accuracy of the predictions of other variables. The accuracy of SWC predictions in this study is comparable to that of our previous MEMS grassland study (Zhang et al., 2021), which is another indication of the model's reliability.

3.2.2 | Soil temperature

Soil temperature (ST), together with moisture, is an important driver of soil biological processes, including decomposition. In our grassland study (Zhang et al., 2021), we demonstrated the high quality of the ST predictions. In the present study, the MEMS 2.14 model also accurately predicts the ST at 4-cm depth for the three sites except during winter, when ST is below 0°C (d = 0.96 and $R^2 = 0.93$ for all sites; Table 2; Figures S16–S18). As SOM decomposition in soil slows down to a minimum rate when ST is at or below 0°C (Sierra et al., 2015), there is currently no need to improve the model for the below 0°C temperature predictions effect on SOM decomposition.

TABLE 2 The statistics for model validation.

		ST at 4 cm	SWC at 10 cm	SWC at 25 cm	SWC at 50 cm	SWC at 100 cm
US-Ne1	d	0.96	0.59	0.60	0.57	0.41
	R^2	0.93	0.25	0.20	0.23	0.02
	RRMSE	0.35	0.19	0.15	0.15	0.17
	RMD	-0.18	0.13	0.06	0.10	-0.14
US-Ne2	d	0.96	0.74	0.70	0.47	0.14
	R^2	0.93	0.41	0.46	0.04	0.20
	RRMSE	0.38	0.10	0.12	0.19	0.24
	RMD	-0.20	-0.02	-0.07	-0.13	-0.24
US-Ne3	d	0.96	0.71	0.81	0.75	0.70
	R^2	0.93	0.36	0.47	0.45	0.49
	RRMSE	0.35	0.19	0.11	0.14	0.13
	RMD	-0.20	0.09	-0.04	-0.08	-0.10

Note: The variables are daily values of soil temperature (ST) and soil water content (SWC). US-Ne1 and US-Ne2 are irrigated, while US-Ne3 is rainfed. Abbreviations: RMD, relative mean difference; RRMSE, relative root mean square error.

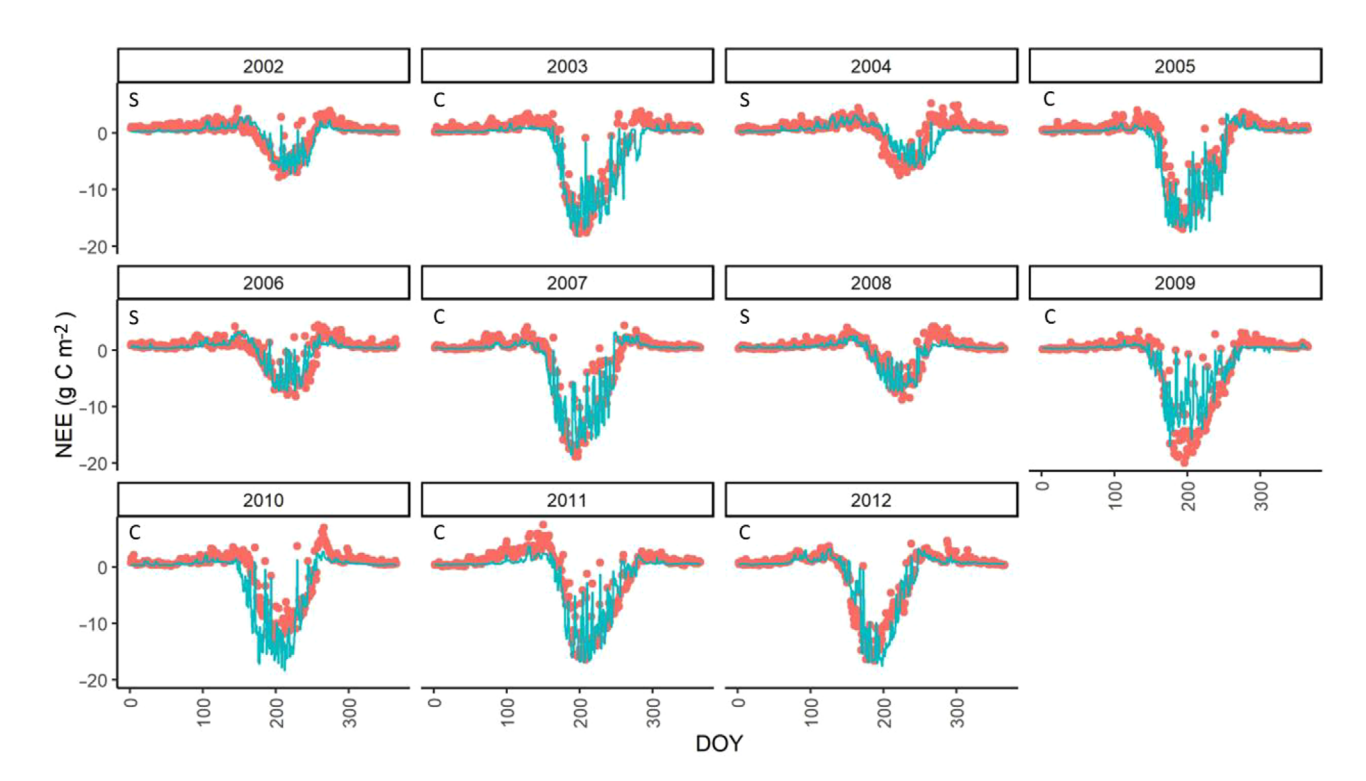


FIGURE 5 Comparison of simulated (lines) and measured (dots) net ecosystem exchange (NEE) at the AmeriFlux US-Ne2 site. DOY, day of year.

3.3 | Net ecosystem exchange

The model captured the seasonal change of NEE for both corn and soybean under both irrigated and rainfed conditions (Figure 5 for US-Ne2 and Figure 6 for US-Ne3; data from US-Ne1 is in Figure S19). Overall, the simulated values are close to the measured with $d \ge 0.90$ and $R^2 \ge 0.73$ (Table 1). During the summer, both photosynthesis and decomposition of organic matter proceed at high rates, consistent with previous

cropland measurements (Lei & Yang, 2010; Soegaard et al., 2003), and in this study, simulated data matched measured data in showing large, negative summer NEE fluxes. During the nongrowing season, while temperatures are warm enough, surface litter and organic matter decomposition contribute to positive NEE fluxes (Baldocchi, 2008; J. Tang et al., 2003). The model tended to underestimate the positive NEE fluxes at the three sites during these periods. This was likely because the model used the temperature at the soil surface (under the

ZHANG ET AL.

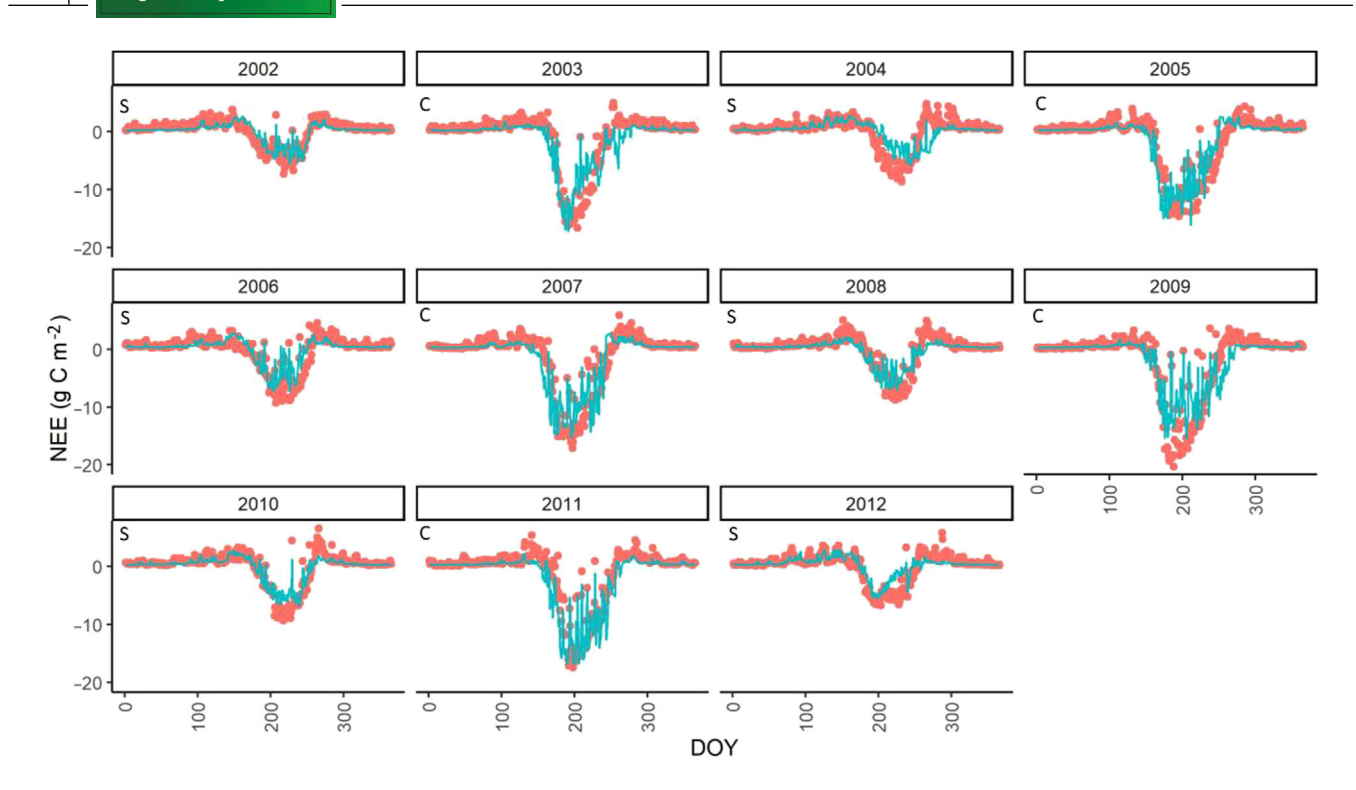


FIGURE 6 Comparison of simulated (lines) and measured (dots) net ecosystem exchange (NEE) at the AmeriFlux US-Ne3 site. DOY, day of year.

litter layer) for litter decomposition rate calculation, rather than air temperature. The temperature at the soil surface does not rapidly warm in response to rising air temperature (due to the insulating effect of surface litter), so the decomposition rate of some of the surface litter on warm days was likely underestimated. Another possibility was that the model does not account for photodegradation, which has been found to significantly accelerate litter decomposition (J. Y. King et al., 2012).

While both the d and R^2 statistics suggest strong agreement between the simulated and measured NEE of soybean at US-Ne3, the RRMSE and RMD were very large. This discrepancy arises primarily due to the low average value of the observations, which acts as the denominator in the calculation of RRMSE and RMD. The observed NEE values range from -9.3 to 6.6, with an average close to zero (-0.0096), attributed to the cancellation effect of positive and negative values. This discrepancy demonstrates the importance of using multiple statistical measures to assess model performance, as reliance on a single index can be misleading. Using NEE to compare against the other indicators of plant productivity can help to evaluate the consistency of model performance between years. For instance, the model's underestimation of crop production in 2009, as shown by NEE values (Figure 5), mirrors the model's underestimation of crop production shown by aboveground biomass (Figure 1) in the same year at the US-Ne2 site. This consistency suggests there was an aspect of the specific corn hybrid used at US-Ne2 in

2009 (different from other years) that was not captured by the model's calibration, but that the model's representation of biomass accumulation and NEE was still internally consistent.

3.4 | Soil organic carbon

The available SOC measurements were values of bulk SOC stock at the 0- to 15-cm and 15- to 30-cm depths at two time points (at site establishment in 2001 and in 2005). The measured SOC in 2001 was quite different between the sites (US-Ne1 has a higher SOC than the other two sites; Figure 7). There was a slight trend for decreasing SOC over the 5-year period between samplings at 0- to 15-cm depth, but the raw data were not available to test if this trend was statistically significant.

The MEMS model predicts SOC stocks for all user-defined soil layers, but here we show only soil layers for which measured data are available (Figure 7). As described in the Methods section, we estimated SOC by first simulating native vegetation and then modeling the land use change to cropland. At these sites, the only available information about the cropland management was that the irrigated sites were under no-till corn—soybean rotation for 10 years before the establishment of the experiments. Regionally appropriate assumptions were made to complete the specific management history for the sites. Using this approach, simulated total SOC values for US-Ne2 were close to the measurements in 2001.

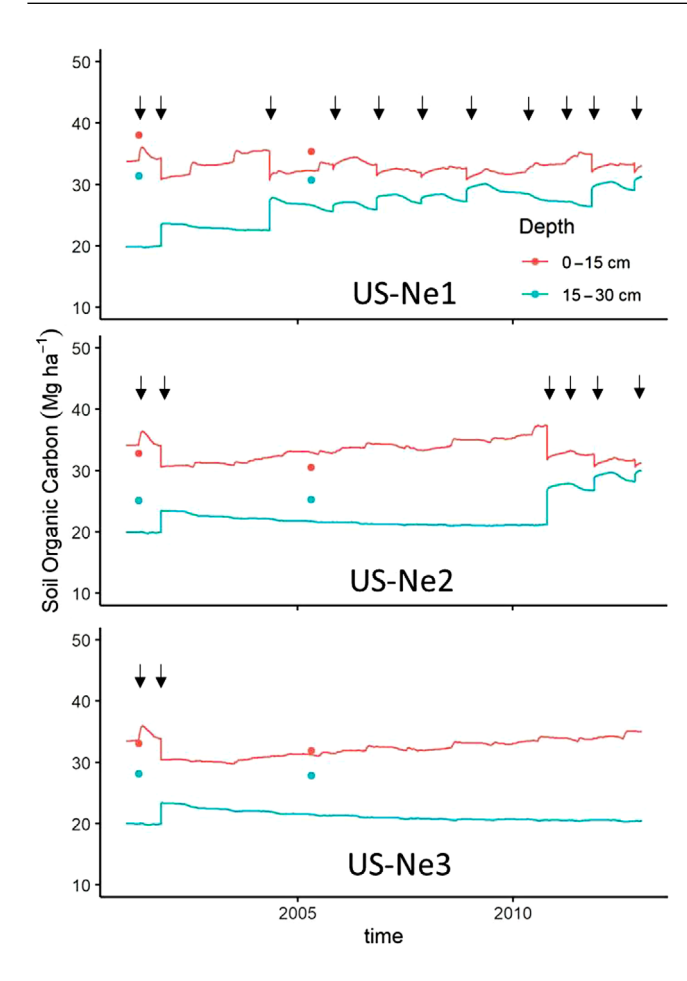


FIGURE 7 Comparison of daily simulated (lines) and measured (dots) soil organic carbon (SOC). The sudden decrease of SOC in the first soil layer and increase of the second soil layer were caused by tillage events (indicated by arrows; different equipment was used). The soil samples corresponding to the first measured data points were taken 1 day after field tillage in April 2001.

Since we used the exact same management history for both US-Ne2 and US-Ne1 sites (they have the same soil type), our SOC estimates were lower than observations for US-Ne1. US-Ne3 used no irrigation, but its SOC values are not much different from the irrigated US-Ne2 for both measured and simulated data. While irrigation increases crop C input to the soil, it also promotes SOC decomposition with higher SWC.

Although the sites used in this study were not designed to test the effect of tillage versus no-till across replicated plots, we can nevertheless observe simulated changes in SOC over time with the introduction of tillage. Tillage events mixed SOC throughout the 0–15 cm and 15–30 cm soil layers (Figure 7), as has been widely documented in field studies (Hernanz et al., 2002; Shi et al., 2011; Zhao et al., 2015). For US-Ne1, the repeated tillage events kept the SOC of the two soil layers very close through the years. In contrast, the absence of tillage at US-Ne3 enabled the predicted SOC of the two layers to differentiate from each other. The observed SOC

values of the two soil layers at US-Ne3 were much closer than the simulated values, which we expect may be due to tillage events in the period prior to the experiment. As historical management is not available for this site, we cannot confirm the reasons for this observation. In addition, the discrepancy between simulated and measured SOC may be attributable to the model's lack of representation of soil aggregation effects, which have been shown to protect SOC from decomposition, discussed in more detail below (Section 3.6).

It is worth noting that only the crop parameters were calibrated in this study. The decomposition-related parameters were the same as those from our grassland simulation (Zhang et al., 2021). Although here we only show the SOC of one specific region, the model performance indicates that the model and its current parameterization have the potential to represent SOC processes under land use change.

3.5 | Soil organic carbon fractions

The SOC fractions (i.e., POC and MAOC) were not measured at the sites used in this study, so we presented the simulated POC and MAOC as an example of model performance relative to expected patterns. Expected patterns in POC and MAOC in the system under study include a decrease of both pools after conversion from native vegetation to agriculture and changes in the percent of MAOC as a component of total SOC (f_{MAOC}). At the US-Ne3 site, under native grassland, the model predicted an f_{MAOC} of 71.0% in the 0–15 cm layer and 92.8% in the 15–30 cm layer (Figure 8). Although f_{MAOC} can vary widely across management systems and soils, these f_{MAOC} percentages are similar to those of the KONZ site (the Konza Prairie) in the same region (less than 300 km in distance) used in our previous study from the National Ecological Observatory Network (Zhang et al., 2021). The f_{MAOC} values measured from a study of global grasslands for the top 10 cm of soil ranged from around 25% to around 90% with an average of 62% (Rocci et al., 2022). Our predicted value of f_{MAOC} for the 0-15 cm layer was thus close to the average of observed values. The simulated POC was more responsive to variability in climate than the simulated MAOC, which was more stable over time. While finely resolved temporal measurements of POC and MAOC are uncommon, the greater vulnerability of POC to climate aligns with findings from previous work (Lugato et al., 2021).

After land use change in 1900 from native grassland to annual grain cropping system with tillage, both MAOC and POC of the 0–15 soil layer dropped due to lower C input and the higher-C surface soil layer mixing with the lower-C 15-30 cm layer, consistent with longer-term studies (Jagadamma & Lal, 2010; Reeder et al., 1998). Over the 50 years from conversion to cropland, the model predicted a gradual loss of MAOC in the 0- to 15-cm depth such that in 1950, the

ZHANG ET AL.

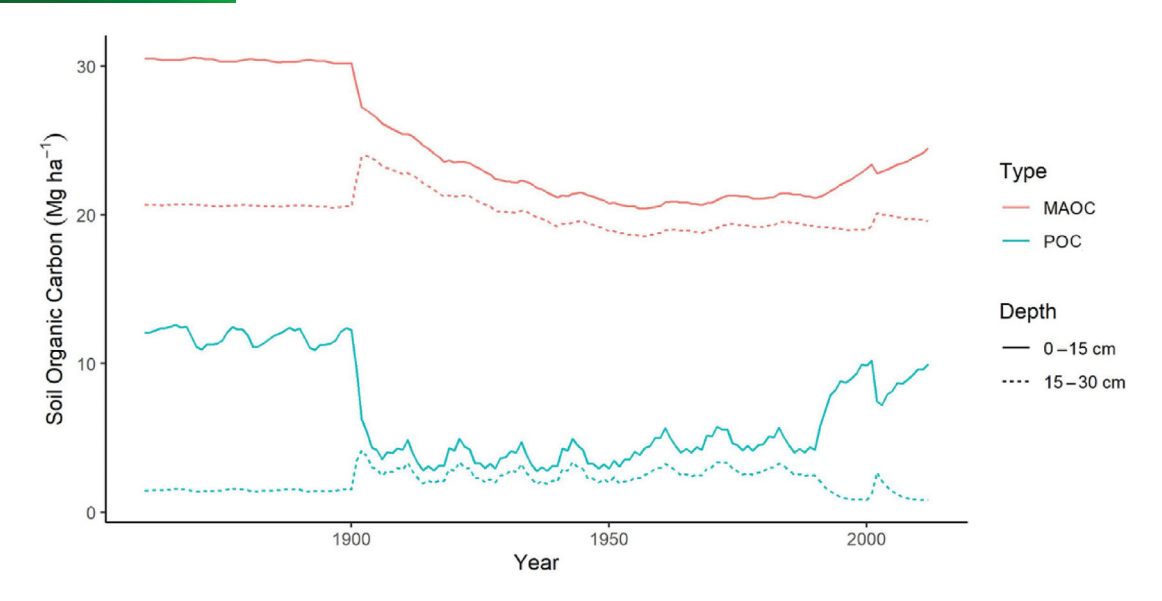


FIGURE 8 The simulated soil carbon in the mineral-associated organic carbon (MAOC) and particulate organic carbon (POC) from 1850 at the AmeriFlux US-Ne3 site. The pre-1900 period was modeled as native grassland. Annual crops and tillage were introduced in 1900. No-till was started in 1990 but the field was tilled in 2001 for experimental preparation.

MAOC pool had lost 31% of its C (from 30.2 to 20.8 Mg ha⁻¹). The model predicted a different dynamic for the POC with a more rapid and bigger (76%) loss of C by 1950 (from $12.4 \text{ to } 3.0 \text{ Mg ha}^{-1}$) compared with 1900 for the 0-15 soil layer (Figure 8). Very contrasting responses were predicted for the subsoil. There was almost no change in MAOC in the 15-30 cm soil layer (20.6 Mg ha⁻¹ in 1900 compared to 18.9 Mg ha⁻¹ in 1950); while POC increased by 29% due to the movement of SOC from the soil layer above through tillage mixing. After 1950, fertilizer was added and there was a slight increase in both SOC pools, especially for POC in the 0–15 cm layer. Overall, the model captured an increase in f_{MAOC} in the surface soil (88% in 1950 in the 0-15) expected under cropland, falling within reported ranges (Beniston et al., 2014; Cambardella & Elliott, 1992; Hansen et al., 2024; A. E. King et al., 2024).

No-till management was introduced in 1990. As a result, the model predicted a big increase of POC in the 0–15 cm (by 5.5 Mg ha⁻¹; from 4.4 to 9.9 Mg ha⁻¹) and a decrease in the 15–30 cm (by 1.7 Mg ha⁻¹; from 2.6 to 0.8 Mg ha⁻¹), which lead to a net increase of 3.8 Mg ha⁻¹ POC in the top 30 cm soil in the year 2000. Regarding MAOC, the implementation of no-till resulted in an increase of 1.9 Mg ha⁻¹ in the 0–15 cm layer and a decrease of 0.3 Mg ha⁻¹ in the 15–30 cm layer (net increase of 1.6 Mg ha⁻¹). Overall, the SOC stock increased by 11% (5.4 Mg C ha⁻¹) across the top 30 cm, after conversion to no-till. This increase of SOC is supported by the general consensus that no-till increases SOC in the topsoil (Luo et al., 2010; Nunes et al., 2020).

3.6 | Limitations, data needs, and future work

Agroecosystem models take a variety of approaches to simulating tillage as a management event and its effects on SOC pools. Almost all models simulate the incorporation of residues and mixing of soil throughout the tillage layer (Maharjan et al., 2018), which MEMS 2.14 also simulates, with default mixing efficiencies defined by the category of tillage operation. Tillage is also often assumed to accelerate decomposition rates, which some models represent by temporarily increasing decomposition constants following a tillage event (Gurung et al., 2020; Porter et al., 2010). The underlying mechanism justifying this approach has been that tillage destroys soil aggregates, which normally protect SOC, as evidenced by several studies (Elliott & Coleman, 1988; A. E. King et al., 2019; Six et al., 2004; Six & Paustian, 2014). However, very few models have taken approaches to explicitly represent aggregation and its effect on decomposition (Laub et al., 2023; Maharjan et al., 2018; Segoli et al., 2013), possibly due to conceptual challenges or constraints on available data. We are working on a new conceptualization of soil aggregation formation and its effect on decomposition and will incorporate it in the next version of the MEMS model.

In this study, we demonstrated the updated MEMS 2.14 model's ability to simulate key ecosystem properties for croplands. However, the available datasets for our study sites lack sufficient data for comprehensive model validation, especially

for SOC and pool distribution. The absence of long-term SOC measurements prevented validating the accuracy of simulated SOC change rates after no-till adoption. While MEMS also simulates deep soil and POC and MAOC fractions throughout the soil profile, we could not evaluate these model aspects without these measurements at the study sites. The scope of this study focuses on the representation of crop growth and agricultural management. The MEMS model is under continual development and we plan to present further model validation in future studies.

4 | CONCLUSION

The expanded capabilities of MEMS 2.14 now enable simulations of annual grain crops and agricultural practices, greatly increasing its potential applications and providing a platform for model development to predict soil C sequestration. This updated model provides a new tool for forecasting cropland systems and for exploring related scientific questions. Our study demonstrates the model's reliability for crop growth representation through comparisons of simulated and measured aboveground biomass, GLAI, NEE, ET, SWC, and ST for major US grain crops. While further validation is still needed, especially for SOC, we anticipate the MEMS model will aid land management decisions and carbon sequestration estimates.

AUTHOR CONTRIBUTIONS

Yao Zhang: Conceptualization; data curation; formal analysis; methodology; software; validation; visualization; writing—original draft. Alison E. King: Writing—original draft. Emma Hamilton: Software. Francesca Cotrufo: Conceptualization; funding acquisition; supervision; writing—review and editing.

ACKNOWLEDGMENTS

The project was supported with funding from the US DOE Advanced Research Projects Agency-Energy programme (ROOTS project; DE-FOA-00001565), from the NSF DEB (award no. 2016003), and from Shell Inc. (contract no. 4550183252). The authors would like to thank Dr. Keith Paustian and Dr. Stephen Ogle for model development discussions. We thank the researchers of AmeriFlux network for their field data collection efforts. We also thank Dr. Andrew Suyker for providing the field data. Funding for the AmeriFlux data portal was provided by the U.S. Department of Energy Office of Science.

CONFLICT OF INTEREST STATEMENT

The authors declare no conflicts of interest.

ORCID

Yao Zhang https://orcid.org/0000-0002-2669-1378

REFERENCES

- Abrahamsen, P., & Hansen, S. (2000). Daisy: An open soil-cropatmosphere system model. *Environmental Modelling & Software*, 15(3), 313–330. https://doi.org/10.1016/S1364-8152(00)00003-7
- Abramoff, R. Z., Guenet, B., Zhang, H., Georgiou, K., Xu, X., Viscarra Rossel, R. A., Yuan, W., & Ciais, P. (2022). Improved global-scale predictions of soil carbon stocks with Millennial version 2. *Soil Biology and Biochemistry*, 164, 108466. https://doi.org/10.1016/j.soilbio. 2021.108466
- Allen, R. G., Pereira, L. S., Raes, D., & Smith, M. (1998). Crop evapotranspiration: Guidelines for computing crop water requirements (Irrigation and Drainage Paper no. 56). FAO.
- Amelung, W., Bossio, D., De Vries, W., Kögel-Knabner, I., Lehmann, J., Amundson, R., Bol, R., Collins, C., Lal, R., Leifeld, J., Minasny, B., Pan, G., Paustian, K., Rumpel, C., Sanderman, J., Van Groenigen, J. W., Mooney, S., Van Wesemael, B., Wander, M., & Chabbi, A. (2020). Towards a global-scale soil climate mitigation strategy. *Nature Communications*, 11(1), 5427. https://doi.org/10.1038/s41467-020-18887-7
- Amiri, E., Irmak, S., & Araji, H. A. (2022). Assessment of CERES-Maize model in simulating maize growth, yield and soil water content under rainfed, limited and full irrigation. *Agricultural Water Management*, 259, 107271. https://doi.org/10.1016/j.agwat.2021.107271
- Archontoulis, S. V., Miguez, F. E., & Moore, K. J. (2014). Evaluating APSIM maize, soil water, soil nitrogen, manure, and soil temperature modules in the Midwestern United States. *Agronomy Journal*, 106(3), 1025–1040. https://doi.org/10.2134/agronj2013.0421
- Babel, M. S., Deb, P., & Soni, P. (2019). Performance evaluation of AquaCrop and DSSAT-CERES for maize under different irrigation and manure application rates in the Himalayan region of India. *Agricultural Research*, 8(2), 207–217. https://doi.org/10.1007/s40003-018-0366-y
- Bagnall, D. K., Morgan, C. L. S., Cope, M., Bean, G. M., Cappellazzi,
 S., Greub, K., Liptzin, D., Norris, C. L., Rieke, E., Tracy, P., Aberle,
 E., Ashworth, A., Bañuelos Tavarez, O., Bary, A., Baumhardt, R.
 L., Borbón Gracia, A., Brainard, D., Brennan, J., Reyes, D. B., &
 Honeycutt, C. W. (2022). Carbon-sensitive pedotransfer functions for
 plant available water. Soil Science Society of America Journal, 86,
 612–629. https://doi.org/10.1002/saj2.20395
- Baldocchi, D. (2008). 'Breathing' of the terrestrial biosphere: Lessons learned from a global network of carbon dioxide flux measurement systems. *Australian Journal of Botany*, *56*(1), 1–26. https://doi.org/10.1071/BT07151
- Basso, B., Ritchie, J. T., Grace, P. R., & Sartori, L. (2006). Simulation of tillage systems impact on soil biophysical properties using the SALUS model. *Italian Journal of Agronomy*, 1(4), 677–688. https://doi.org/10.4081/ija.2006.677
- Beniston, J. W., Dupont, S. T., Glover, J. D., Lal, R., & Dungait, J. A. J. (2014). Soil organic carbon dynamics 75 years after land-use change in perennial grassland and annual wheat agricultural systems. *Biogeochemistry*, 120(1), 37–49. https://doi.org/10.1007/s10533-014-9980-3
- Brooks, R. H., & Corey, A. T. (1964). *Hydraulic properties of porous media* (Hydrology Paper no. 3). Colorado State University.

- Cambardella, C. A., & Elliott, E. T. (1992). Particulate soil organic-matter changes across a grassland cultivation sequence. *Soil Science Society of America Journal*, 56(3), 777–783. https://doi.org/10.2136/sssaj1992.03615995005600030017x
- Coleman, K., & Jenkinson, D. S. (1996). RothC-26.3—A model for the turnover of carbon in soil. In D. S. Powlson, P. Smith, & J. U. Smith (Eds.), *Evaluation of soil organic matter models* (pp. 237–246). Springer.
- Cotrufo, M. F., & Lavallee, J. M. (2022). Soil organic matter formation, persistence, and functioning: A synthesis of current understanding to inform its conservation and regeneration. In D. L. Sparks (Ed.), *Advances in agronomy* (pp. 1–66). Academic Press.
- Cotrufo, M. F., Ranalli, M. G., Haddix, M. L., Six, J., & Lugato, E. (2019). Soil carbon storage informed by particulate and mineral-associated organic matter. *Nature Geoscience*, 12(12), 989–994. https://doi.org/10.1038/s41561-019-0484-6
- Cotrufo, M. F., Soong, J. L., Horton, A. J., Campbell, E. E., Haddix, M. L., Wall, D. H., & Parton, W. J. (2015). Formation of soil organic matter via biochemical and physical pathways of litter mass loss. *Nature Geoscience*, 8(10), 776–779. https://doi.org/10.1038/ngeo2520
- Cotrufo, M. F., Wallenstein, M. D., Boot, C. M., Denef, K., & Paul, E. (2013). The microbial efficiency-matrix stabilization (MEMS) framework integrates plant litter decomposition with soil organic matter stabilization: Do labile plant inputs form stable soil organic matter? Global Change Biology, 19(4), 988–995. https://doi.org/10.1111/gcb. 12113
- Crippa, M., Solazzo, E., Guizzardi, D., Monforti-Ferrario, F., Tubiello, F. N., & Leip, A. (2021). Food systems are responsible for a third of global anthropogenic GHG emissions. *Nature Food*, 2(3), 198–209. https://doi.org/10.1038/s43016-021-00225-9
- Dondini, M., Hastings, A., Saiz, G., Jones, M. B., & Smith, P. (2009). The potential of Miscanthus to sequester carbon in soils: Comparing field measurements in Carlow, Ireland to model predictions. *GCB Bioenergy*, 1(6), 413–425. https://doi.org/10.1111/j.1757-1707.2010.01033.x
- Elliott, E. T., & Coleman, D. C. (1988). Let the soil work for us. *Ecological Bulletins*, 39, 23–32.
- FAOSTAT. (2021). Food and agriculture data. https://www.fao.org/faostat
- Fowler, D. B., Byrns, B. M., & Greer, K. J. (2014). Overwinter low-temperature responses of cereals: Analyses and simulation. *Crop Science*, 54(6), 2395–2405. https://doi.org/10.2135/cropsci2014.03. 0196
- Franzluebbers, A. J. (2002). Water infiltration and soil structure related to organic matter and its stratification with depth. *Soil and Tillage Research*, 66(2), 197–205. https://doi.org/10.1016/S0167-1987(02) 00027-2
- Friend, A. D., Arneth, A., Kiang, N. Y., Lomas, M., Ogée, J., Rödenbeck, C., Running, S. W., Santaren, J.-D., Sitch, S., Viovy, N., Ian Woodward, F., & Zaehle, S. (2007). FLUXNET and modelling the global carbon cycle. *Global Change Biology*, 13(3), 610–633. https://doi.org/10.1111/j.1365-2486.2006.01223.x
- Grant, R. F., Arkebauer, T. J., Dobermann, A., Hubbard, K. G., Schimelfenig, T. T., Suyker, A. E., Verma, S. B., & Walters, D. T. (2007). Net biome productivity of irrigated and rainfed maize–soybean rotations: Modeling vs. measurements. *Agron-omy Journal*, 99(6), 1404–1423. https://doi.org/10.2134/agronj2006. 0308

- Guo, L. B., & Gifford, R. M. (2002). Soil carbon stocks and land use change: A meta analysis. *Global Change Biology*, 8(4), 345–360. https://doi.org/10.1046/j.1354-1013.2002.00486.x
- Gurung, R. B., Ogle, S. M., Breidt, F. J., Williams, S. A., & Parton, W. J. (2020). Bayesian calibration of the DayCent ecosystem model to simulate soil organic carbon dynamics and reduce model uncertainty. *Geoderma*, 376, 114529. https://doi.org/10.1016/j.geoderma. 2020.114529
- Hanan, N. P., Burba, G., Verma, S. B., Berry, J. A., Suyker, A., & Walter-Shea, E. A. (2002). Inversion of net ecosystem CO₂ flux measurements for estimation of canopy PAR absorption. *Global Change Biology*, 8(6), 563–574. https://doi.org/10.1046/j.1365-2486. 2002.00488.x
- Hansen, P. M., Even, R., King, A. E., Lavallee, J., Schipanski, M., & Cotrufo, M. F. (2024). Distinct, direct and climate-mediated environmental controls on global particulate and mineral-associated organic carbon storage. *Global Change Biology*, 30(1), e17080. https://doi.org/10.1111/gcb.17080
- Hargreaves, G. H., & Allen, R. G. (2003). History and evaluation of Hargreaves evapotranspiration equation. *Journal of Irrigation and Drainage Engineering*, 129, 53–63. https://doi.org/10.1061/(ASCE) 0733-9437(2003)129:1(53)
- Hernanz, J. L., López, R., Navarrete, L., & Sánchez-Girón, V. (2002). Long-term effects of tillage systems and rotations on soil structural stability and organic carbon stratification in semiarid central Spain. Soil and Tillage Research, 66(2), 129–141. https://doi.org/10.1016/ S0167-1987(02)00021-1
- Jagadamma, S., & Lal, R. (2010). Distribution of organic carbon in physical fractions of soils as affected by agricultural management. *Biology and Fertility of Soils*, 46(6), 543–554. https://doi.org/10. 1007/s00374-010-0459-7
- Janzen, H. H. (2004). Carbon cycling in earth systems—A soil science perspective. Agriculture, Ecosystems & Environment, 104(3), 399–417. https://doi.org/10.1016/j.agee.2004.01.040
- Jones, J. W., Hoogenboom, G., Porter, C. H., Boote, K. J., Batchelor, W. D., Hunt, L. A., Wilkens, P. W., Singh, U., Gijsman, A. J., & Ritchie, J. T. (2003). The DSSAT cropping system model. *European Journal of Agronomy*, 18(3), 235–265. https://doi.org/10.1016/S1161-0301(02) 00107-7
- Keating, B. A., Carberry, P. S., Hammer, G. L., Probert, M. E., Robertson, M. J., Holzworth, D., Huth, N. I., Hargreaves, J. N. G., Meinke, H., Hochman, Z., Mclean, G., Verburg, K., Snow, V., Dimes, J. P., Silburn, M., Wang, E., Brown, S., Bristow, K. L., Asseng, S., ... Smith, C. J. (2003). An overview of APSIM, a model designed for farming systems simulation. *European Journal of Agronomy*, 18(3), 267–288. https://doi.org/10.1016/S1161-0301(02)00108-9
- King, A. E., Amsili, J. P., Córdova, S. C., Culman, S., Fonte, S. J., Kotcon, J., Masters, M. D., McVay, K., Olk, D. C., Prairie, A. M., Schipanski, M., Schneider, S. K., Stewart, C. E., & Cotrufo, M. F. (2024). Constraints on mineral-associated and particulate organic carbon response to regenerative management: Carbon inputs and saturation deficit. *Soil and Tillage Research*, 238, 106008. https://doi. org/10.1016/j.still.2024.106008
- King, A. E., Congreves, K. A., Deen, B., Dunfield, K. E., Voroney, R. P., & Wagner-Riddle, C. (2019). Quantifying the relationships between soil fraction mass, fraction carbon, and total soil carbon to assess mechanisms of physical protection. *Soil Biology and Biochemistry*, 135, 95–107. https://doi.org/10.1016/j.soilbio.2019.04.019

- King, J. Y., Brandt, L. A., & Adair, E. C. (2012). Shedding light on plant litter decomposition: Advances, implications and new directions in understanding the role of photodegradation. *Biogeochemistry*, 111(1), 57–81, https://doi.org/10.1007/s10533-012-9737-9
- Kleber, M., Sollins, P., & Sutton, R. (2007). A conceptual model of organo-mineral interactions in soils: Self-assembly of organic molecular fragments into zonal structures on mineral surfaces. *Biogeochemistry*, 85(1), 9–24. https://doi.org/10.1007/s10533-007-9103-5
- Kollas, C., Kersebaum, K. C., Nendel, C., Manevski, K., Müller, C., Palosuo, T., Armas-Herrera, C. M., Beaudoin, N., Bindi, M., Charfeddine, M., Conradt, T., Constantin, J., Eitzinger, J., Ewert, F., Ferrise, R., Gaiser, T., de Cortazar-Atauri, I. G., Giglio, L., Hlavinka, P., ... Wu, L. (2015). Crop rotation modelling—A European model intercomparison. *European Journal of Agronomy*, 70, 98–111. https://doi.org/10.1016/j.eja.2015.06.007
- Lal, R., Smith, P., Jungkunst, H. F., Mitsch, W. J., Lehmann, J., Nair, P. K. R., Mcbratney, A. B., De Moraes Sá, J. C., Schneider, J., Zinn, Y. L., Skorupa, A. L. A., Zhang, H.-L., Minasny, B., Srinivasrao, C., & Ravindranath, N. H. (2018). The carbon sequestration potential of terrestrial ecosystems. *Journal of Soil and Water Conservation*, 73(6), 145A–152A. https://doi.org/10.2489/jswc.73.6.145A
- Laub, M., Blagodatsky, S., Van de Broek, M., Schlichenmaier, S., Kunlanit, B., Six, J., Vityakon, P., & Cadisch, G. (2023). SAMM version 1.0: A numerical model for microbial mediated soil aggregate formation. EGUsphere, https://doi.org/10.5194/egusphere-2023-1414
- Launay, C., Constantin, J., Chlebowski, F., Houot, S., Graux, A.-I., Klumpp, K., Martin, R., Mary, B., Pellerin, S., & Therond, O. (2021). Estimating the carbon storage potential and greenhouse gas emissions of French arable cropland using high-resolution modeling. *Global Change Biology*, 27(8), 1645–1661. https://doi.org/10.1111/ gcb.15512
- Lei, H.-M., & Yang, D.-W. (2010). Seasonal and interannual variations in carbon dioxide exchange over a cropland in the North China Plain. *Global Change Biology*, *16*(11), 2944–2957. https://doi.org/10.1111/j.1365-2486.2009.02136.x
- Li, C., Frolking, S., & Frolking, T. A. (1992). A model of nitrous oxide evolution from soil driven by rainfall events: 1. Model structure and sensitivity. *Journal of Geophysical Research: Atmospheres*, 97(D9), 9759–9776. https://doi.org/10.1029/92JD00509
- Liang, C., Schimel, J. P., & Jastrow, J. D. (2017). The importance of anabolism in microbial control over soil carbon storage. *Nature Microbiology*, 2(8), 17105. https://doi.org/10.1038/nmicrobiol.2017. 105
- Lugato, E., Bampa, F., Panagos, P., Montanarella, L., & Jones, A. (2014). Potential carbon sequestration of European arable soils estimated by modelling a comprehensive set of management practices. Global Change Biology, 20(11), 3557–3567. https://doi.org/10.1111/gcb.12551
- Lugato, E., Lavallee, J. M., Haddix, M. L., Panagos, P., & Cotrufo, M. F. (2021). Different climate sensitivity of particulate and mineral-associated soil organic matter. *Nature Geoscience*, 14(5), 295–300. https://doi.org/10.1038/s41561-021-00744-x
- Luo, Z., Wang, E., & Sun, O. J. (2010). Can no-tillage stimulate carbon sequestration in agricultural soils? A meta-analysis of paired experiments. *Agriculture, Ecosystems & Environment*, 139(1), 224–231. https://doi.org/10.1016/j.agee.2010.08.006

- Maharjan, G. R., Prescher, A.-K., Nendel, C., Ewert, F., Mboh, C. M., Gaiser, T., & Seidel, S. J. (2018). Approaches to model the impact of tillage implements on soil physical and nutrient properties in different agro-ecosystem models. *Soil and Tillage Research*, 180, 210–221. https://doi.org/10.1016/j.still.2018.03.009
- Marek, G. W., Marek, T. H., Xue, Q., Gowda, P. H., Evett, S. R., & Brauer, D. K. (2017). Simulating evapotranspiration and yield response of selected corn varieties under full and limited irrigation in the Texas High Plains using DSSAT-CERES-maize. *Transactions* of the ASABE, 60(3), 837–846. https://doi.org/10.13031/trans.12048
- Novick, K. A., Biederman, J. A., Desai, A. R., Litvak, M. E., Moore, D. J. P., Scott, R. L., & Torn, M. S. (2018). The AmeriFlux network: A coalition of the willing. *Agricultural and Forest Meteorology*, 249, 444–456. https://doi.org/10.1016/j.agrformet.2017.10.009
- Nunes, M. R., Karlen, D. L., Veum, K. S., Moorman, T. B., & Cambardella, C. A. (2020). Biological soil health indicators respond to tillage intensity: A US meta-analysis. *Geoderma*, 369, 114335. https://doi.org/10.1016/j.geoderma.2020.114335
- Oldfield, E. E., Bradford, M. A., & Wood, S. A. (2019). Global metaanalysis of the relationship between soil organic matter and crop yields. *Soil*, 5(1), 15–32. https://doi.org/10.5194/soil-5-15-2019
- Oldfield, E. E., Eagle, A. J., Rubin, R. L., Rudek, J., Sanderman, J., & Gordon, D. R. (2022). Crediting agricultural soil carbon sequestration. *Science*, *375*(6586), 1222–1225. https://doi.org/10.1126/science.abl7991
- Parton, W. J., Hartman, M., Ojima, D., & Schimel, D. (1998). DAY-CENT and its land surface submodel: Description and testing. *Global and Planetary Change*, 19(1), 35–48. https://doi.org/10.1016/S0921-8181(98)00040-X
- Parton, W. J., Schimel, D. S., Cole, C. V., & Ojima, D. S. (1987). Analysis of factors controlling soil organic matter levels in Great Plains grasslands. *Soil Science Society of America Journal*, *51*(5), 1173–1179. https://doi.org/10.2136/sssaj1987.03615995005100050015x
- Paustian, K., Lehmann, J., Ogle, S., Reay, D., Robertson, G. P., & Smith, P. (2016). Climate-smart soils. *Nature*, 532(7597), 49–57. https://doi. org/10.1038/nature17174
- Porter, C. H., Jones, J. W., Adiku, S., Gijsman, A. J., Gargiulo, O., & Naab, J. B. (2010). Modeling organic carbon and carbon-mediated soil processes in DSSAT v4.5. *Operational Research: An International Journal*, 10(3), 247–278. https://doi.org/10.1007/s12351-009-0059-1
- Prince, S. D., Haskett, J., Steininger, M., Strand, H., & Wright, R. (2001). Net primary production of U.S. Midwest croplands from agricultural harvest yield data. *Ecological Applications*, 11(4), 1194–1205. https://doi.org/10.1890/1051-0761(2001)011% 5b1194:NPPOUS%5d2.0.CO;2
- Raes, D., Steduto, P., Hsiao, T. C., & Fereres, E. (2009). AquaCrop— The FAO crop model to simulate yield response to water: II. Main algorithms and software description. *Agronomy Journal*, 101, 438– 447. https://doi.org/10.2134/agronj2008.0140s
- Ramankutty, N., Evan, A. T., Monfreda, C., & Foley, J. A. (2008). Farming the planet: 1. Geographic distribution of global agricultural lands in the year 2000. *Global Biogeochemical Cycles*, 22(1), GB1003. https://doi.org/10.1029/2007GB002952
- Ramírez, P. B., Calderón, F. J., Haddix, M., Lugato, E., & Cotrufo, M. F. (2021). Using diffuse reflectance spectroscopy as a high throughput method for quantifying soil C and N and their distribution in particulate and mineral-associated organic matter fractions. Frontiers

in Environmental Science, 9, Article 634472. https://doi.org/10.3389/fenvs.2021.634472

- Rassam, D., Šimůnek, J., Mallants, D., & van Genuchten, M. Th. (2018). The HYDRUS-1D software package for simulating the one-dimensional movement of water, heat, and multiple solutes on variably-saturated meda: Tutorial (Version 1.00). CSIRO Land and Water.
- Reeder, J. D., Schuman, G. E., & Bowman, R. A. (1998). Soil C and N changes on conservation reserve program lands in the Central Great Plains. *Soil and Tillage Research*, 47(3), 339–349. https://doi.org/10.1016/S0167-1987(98)00122-6
- Revill, A., Emmel, C., D'odorico, P., Buchmann, N., Hörtnagl, L., & Eugster, W. (2019). Estimating cropland carbon fluxes: A process-based model evaluation at a Swiss crop-rotation site. *Field Crops Research*, 234, 95–106. https://doi.org/10.1016/j.fcr.2019.02.006
- Ritchie, J. R., & Otter, S. (1985). Description and performance of CERES-Wheat: A user-oriented wheat yield model. In ARS wheat yield project (ARS-38, pp. 159–175). Natural Technology Information Service.
- Robertson, A. D., Paustian, K., Ogle, S., Wallenstein, M. D., Lugato, E., & Cotrufo, M. F. (2019). Unifying soil organic matter formation and persistence frameworks: The MEMS model. *Biogeosciences*, 16(6), 1225–1248. https://doi.org/10.5194/bg-16-1225-2019
- Rocci, K. S., Barker, K. S., Seabloom, E. W., Borer, E. T., Hobbie, S. E., Bakker, J. D., Macdougall, A. S., Mcculley, R. L., Moore, J. L., Raynaud, X., Stevens, C. J., & Cotrufo, M. F. (2022). Impacts of nutrient addition on soil carbon and nitrogen stoichiometry and stability in globally-distributed grasslands. *Biogeochemistry*, 159(3), 353–370. https://doi.org/10.1007/s10533-022-00932-w
- Ross, P. J. (2003). Modeling soil water and solute transport—Fast, simplified numerical solutions. *Agronomy Journal*, 95, 1352–1361. https://doi.org/10.2134/agronj2003.1352
- Sanderman, J., Hengl, T., & Fiske, G. J. (2017). Soil carbon debt of 12,000 years of human land use. *PNAS*, 114(36), 9575–9580. https:// doi.org/10.1073/pnas.1706103114
- Saxton, K. E., & Rawls, W. J. (2006). Soil water characteristic estimates by texture and organic matter for hydrologic solutions. *Soil Science Society of America Journal*, 70(5), 1569–1578. https://doi.org/10.2136/sssaj2005.0117
- Segoli, M., De Gryze, S., Dou, F., Lee, J., Post, W. M., Denef, K., & Six, J. (2013). AggModel: A soil organic matter model with measurable pools for use in incubation studies. *Ecological Modelling*, 263, 1–9. https://doi.org/10.1016/j.ecolmodel.2013.04.010
- Shi, X., Yang, X., Drury, C. F., Reynolds, W. D., Mclaughlin, N. B., Welacky, T. W., & Zhang, X. (2011). Zone tillage impacts on organic carbon of a clay loam in Southwestern Ontario. *Soil Science Society of America Journal*, 75(3), 1083–1089. https://doi.org/10.2136/sssaj2010.0319
- Sierra, C. A., Trumbore, S. E., Davidson, E. A., Vicca, S., & Janssens, I. (2015). Sensitivity of decomposition rates of soil organic matter with respect to simultaneous changes in temperature and moisture. *Journal* of Advances in Modeling Earth Systems, 7(1), 335–356. https://doi. org/10.1002/2014MS000358
- Six, J., Bossuyt, H., Degryze, S., & Denef, K. (2004). A history of research on the link between (micro)aggregates, soil biota, and soil organic matter dynamics. *Soil and Tillage Research*, 79(1), 7–31. https://doi.org/10.1016/j.still.2004.03.008
- Six, J., & Paustian, K. (2014). Aggregate-associated soil organic matter as an ecosystem property and a measurement tool. Soil Biology and

- Biochemistry, 68, A4–A9. https://doi.org/10.1016/j.soilbio.2013.06.
- Soares, M., & Rousk, J. (2019). Microbial growth and carbon use efficiency in soil: Links to fungal-bacterial dominance, SOC-quality and stoichiometry. *Soil Biology and Biochemistry*, 131, 195–205. https://doi.org/10.1016/j.soilbio.2019.01.010
- Soegaard, H. (2003). Carbon dioxide exchange over agricultural landscape using eddy correlation and footprint modelling. *Agricultural* and Forest Meteorology, 114(3), 153–173. https://doi.org/10.1016/ S0168-1923(02)00177-6
- Sokol, N. W., Sanderman, J., & Bradford, M. A. (2019). Pathways of mineral-associated soil organic matter formation: Integrating the role of plant carbon source, chemistry, and point of entry. *Global Change Biology*, 25(1), 12–24. https://doi.org/10.1111/gcb.14482
- Soltani, A., & Sinclair, T. R. (2012). Modeling physiology of crop development, growth and yield. CABI.
- Steduto, P., Hsiao, T. C., Raes, D., & Fereres, E. (2009). AquaCrop—The FAO crop model to simulate yield response to water: I. Concepts and underlying principles. *Agronomy Journal*, 101(3), 426–437. https://doi.org/10.2134/agronj2008.0139s
- Stöckle, C. O., Donatelli, M., & Nelson, R. (2003). CropSyst, a cropping systems simulation model. *European Journal of Agronomy*, *18*(3), 289–307. https://doi.org/10.1016/S1161-0301(02)00109-0
- Sulman, B. N., Brzostek, E. R., Medici, C., Shevliakova, E., Menge, D. N. L., & Phillips, R. P. (2017). Feedbacks between plant N demand and rhizosphere priming depend on type of mycorrhizal association. *Ecology Letters*, 20(8), 1043–1053. https://doi.org/10.1111/ele.12802
- Suyker, A. (2023a). AmeriFlux BASE US-Ne1 Mead irrigated continuous maize site (Version 14-5) [Dataset]. AmeriFlux Management Project, U.S. Department of Energy. https://doi.org/10.17190/AMF/ 1246084
- Suyker, A. (2023b). AmeriFlux BASE US-Ne2 Mead irrigated maizesoybean rotation site (Version 14-5) [Dataset]. AmeriFlux Management Project, U.S. Department of Energy. https://doi.org/10.17190/ AMF/1246085
- Suyker, A. (2023c). AmeriFlux BASE US-Ne3 Mead rainfed maizesoybean rotation site (Version 14-5) [Dataset]. AmeriFlux Management Project, U.S. Department of Energy. https://doi.org/10.17190/ AMF/1246086
- Suyker, A. E., & Verma, S. B. (2009). Evapotranspiration of irrigated and rainfed maize–soybean cropping systems. *Agricultural and Forest Meteorology*, 149(3), 443–452. https://doi.org/10.1016/j.agrformet. 2008.09.010
- Tang, F. H. M., Riley, W. J., & Maggi, F. (2019). Hourly and daily rainfall intensification causes opposing effects on C and N emissions, storage, and leaching in dry and wet grasslands. *Biogeochemistry*, 144(2), 197–214. https://doi.org/10.1007/s10533-019-00580-7
- Tang, J., Baldocchi, D. D., Qi, Y., & Xu, L. (2003). Assessing soil CO2 efflux using continuous measurements of CO2 profiles in soils with small solid-state sensors. *Agricultural and Forest Meteorology*, 118(3), 207–220. https://doi.org/10.1016/S0168-1923(03)00112-6
- Tifafi, M., Camino-Serrano, M., Hatté, C., Morras, H., Moretti, L., Barbaro, S., Cornu, S., & Guenet, B. (2018). The use of radiocarbon ¹⁴C to constrain carbon dynamics in the soil module of the land surface model ORCHIDEE (SVN r5165). *Geoscientific Model Development*, https://doi.org/10.5194/gmd-2018-102
- Vandenbygaart, A. J., Bremer, E., Mcconkey, B. G., Ellert, B. H., Janzen, H. H., Angers, D. A., Carter, M. R., Drury, C. F., Lafond, G. P., & Mckenzie, R. H. (2011). Impact of sampling depth on differences in

- soil carbon stocks in long-term agroecosystem experiments. *Soil Science Society of America Journal*, 75(1), 226–234. https://doi.org/10.2136/sssaj2010.0099
- Verma, S. (2016). AmeriFlux BASE US-Pon Ponca City (Version 2-1) [Dataset]. AmeriFlux Management Project, U.S. Department of Engery. https://doi.org/10.17190/AMF/1246091
- Wang, G., Huang, W., Zhou, G., Mayes, M. A., & Zhou, J. (2020).
 Modeling the processes of soil moisture in regulating microbial and carbon-nitrogen cycling. *Journal of Hydrology*, 585, 124777. https://doi.org/10.1016/j.jhydrol.2020.124777
- Wieder, W. R., Grandy, A. S., Kallenbach, C. M., & Bonan, G. B. (2014). Integrating microbial physiology and physio-chemical principles in soils with the MIcrobial-MIneral Carbon Stabilization (MIMICS) model. *Biogeosciences*, 11(14), 3899–3917. https://doi.org/10.5194/ bg-11-3899-2014
- Williams, J. R., & Izaurralde, R. C. (2010). The APEX model. In *Watershed models* (pp. 461–506). CRC Press.
- Wolf, J. (2012). User guide for LINTUL5: Simple generic model for simulation of crop growth under potential, water limited and nitrogen, phosphorus and potassium limited conditions. Wageningen University.
- Woolf, D., & Lehmann, J. (2019). Microbial models with minimal mineral protection can explain long-term soil organic carbon persistence. Scientific Reports, 9(1), 6522. https://doi.org/10.1038/s41598-019-43026-8
- Yin, X., & van Laar, H. H. (2005). Crop systems dynamics: An ecophysiological simulation model for genotype-by-environment interactions. Wageningen Academic Publishers.
- Yu, L., Ahrens, B., Wutzler, T., Schrumpf, M., & Zaehle, S. (2020). Jena soil model (JSM v1.0; revision 1934): A microbial soil organic carbon model integrated with nitrogen and phosphorus processes. *Geosci*entific Model Development, 13(2), 783–803. https://doi.org/10.5194/ gmd-13-783-2020
- Zhang, Y., Gurung, R., Marx, E., Williams, S., Ogle, S. M., & Paustian, K. (2020). DayCent model predictions of NPP and grain yields for agricultural lands in the contiguous U.S. *Journal of Geophysical*

- Research: Biogeosciences, 125(7), e2020JG005750. https://doi.org/10.1029/2020JG005750
- Zhang, Y., Hansen, N., Trout, T., Nielsen, D., & Paustian, K. (2018). Modeling deficit irrigation of maize with the DayCent model. Agronomy Journal, 110(5), 1754–1764. https://doi.org/10.2134/agronj2017.10.0585
- Zhang, Y., Lavallee, J. M., Robertson, A. D., Even, R., Ogle, S. M., Paustian, K., & Cotrufo, M. F (2021). Simulating measurable ecosystem carbon and nitrogen dynamics with the mechanistically defined MEMS 2.0 model. *Biogeosciences*, *18*(10), 3147–3171. https://doi.org/10.5194/bg-18-3147-2021
- Zhang, Y., Suyker, A., & Paustian, K. (2018). Improved crop canopy and water balance dynamics for agroecosystem modeling using Day-Cent. Agronomy Journal, 110(2), 511–524. https://doi.org/10.2134/ agronj2017.06.0328
- Zhao, X., Xue, J.-F., Zhang, X.-Q., Kong, F.-L., Chen, F., Lal, R., & Zhang, H.-L. (2015). Stratification and storage of soil organic carbon and nitrogen as affected by tillage practices in the North China Plain. *PLoS One*, 10(6), e0128873. https://doi.org/10.1371/journal.pone.0128873

SUPPORTING INFORMATION

Additional supporting information can be found online in the Supporting Information section at the end of this article.

How to cite this article: Zhang, Y., King, A. E., Hamilton, E., & Cotrufo, M. F. (2024). Representing cropping systems with the MEMS 2 ecosystem model. *Agronomy Journal*, *116*, 2328–2345. https://doi.org/10.1002/agj2.21611